Received November 30, 2017, accepted December 24, 2017, date of publication January 1, 2018, date of current version March 9, 2018.

Digital Object Identifier 10.1109/ACCESS.2017.2788400

Modeling and Self-Learning Soft-Grasp Control for Free-Floating Space Manipulator During Target Capturing Using Variable Stiffness Method

MING CHU AND XINGYU WU

Automation School, Beijing University of Posts and Telecommunications, Beijing 100876, China

Corresponding author: Xingyu Wu (wuxingyu1012@163.com)

This work was supported by the National Natural Science Foundation of China under Grant 51305039.

ABSTRACT During target capturing operation, the changes in the dynamics parameters of a free-floating space manipulator degrade the performance of the base attitude stabilization. This paper presents a new self-learning soft-grasp control algorithm based on the variable stiffness technology. First, the dynamic model of variable stiffness joint space manipulator system is established. Simultaneously, the detailed dynamic analysis of pre-impact and post-impact stages is carried out. Second, a new soft-grasp control strategy utilizing cellular differential evolution algorithm combined opposition-based learning with orthogonal crossover is employed to minimize the base angular momentum. Its principle is to solve the optimal stiffness value of the variable stiffness joint to realize desired buffering. Thereafter, we put forward an adaptive backstepping sliding mode control method to track the actual joint stiffness. Finally, the proposed method is applied to a two-degree of freedom planar free-floating space manipulator and the simulation results verify the effectiveness.

INDEX TERMS Coupling angular momentum, post-impact control, variable stiffness, cellular differential evolution, adaptive backstepping.

I. INTRODUCTION

Space robotics is considered one of the most promising approaches for on-orbit servicing missions such as docking, berthing, repairing, upgrading, transporting, rescuing, and orbital debris removal [1]. When space robots accomplish above tasks, they need to capture the resting or moving targets. The main difference between the space robot and the ground robot is that the space robot base is not fixed and there exists the kinematics and dynamics coupling between the manipulator and the base. As a result, it is more difficult for space robots to capture targets. Apart from this, the impulse will influence the momentum of the system, introduce the additional angular momentum to the base, which may lead to the whole system rolling over. At this moment, the disturbance may cause the reaction wheel saturation or seriously affect the quality of communication [2].

Therefore, many scholars have studied on how to reduce the disturbance of the base attitude. Generally, a capturing task consists of three specific phases: the pre-impact phase, the impact phase and the post-impact phase. The impulse brought by the impact phase makes the first phase and the third phase discontinuous. For this problem, Yoshida *et al.*[3] first proposed the Extended Generalized Inertia Tensor (Ex-GIT) and virtual mass concepts. Based on the concepts, they formulated the basic collision dynamics for the free-floating multi-body system regardless of the changes of collision force, but considering the momentum conservation law. Subsequently, they put forward the concept Extended Inversed Inertia Tensor (Ex-IIT) [4] and applied which to impulse minimization. Though they minimized the impulse by means of the concept, it related to the collision direction and link postures, which was hard to control. Also from the viewpoint of the force impulse generated during the contact, a gradient projection algorithm that achieved both trajectory tracking and impulse minimization was proposed by Wee and Walker [5].

From the view of the angular momentum, reaction null-space control and impedance matching control are introduced by Nenchev and Yoshida [6], [7] and Yoshida and Nakanishi [8] to reduce the attitude disturbance to the base body. They also found that preferable directions of the force impulse exist, such that the impact would not change the angular momentum of the space robot. Based on this idea, a straight arm capture concept introduced in [9],

2169-3536 © 2018 IEEE. Translations and content mining are permitted for academic research only.
Personal use is also permitted, but republication/redistribution requires IEEE permission.
See http://www.ieee.org/publications_standards/publications/rights/index.html for more information.

namely all centroids of the links and the base were on the same line, and the force impulse direction was along that line. The posture was so special that it was difficult for space robot to achieve. By using the reaction null space, Dimitrov and Yoshida [10] put forward the method of preloading bias angular momentum in the chaser's base and manipulator arm. They focused on the momentum distribution in the chaser satellite during approaching and post-impact phase and applied distributed momentum control [11] and reaction null space control on the system after impact. But it needs to estimate the angular momentum of the target. On the basis of bias momentum approach, a concept of zero disturbance direction was raised in [12]. In [13], under the condition that the maximum racemization damping force is limited, the theory of optimal control and Pontryagin's principle are applied to bring the tumbling non-cooperative satellite to rest in minimum time while ensuring that the magnitude of the interaction torque between the manipulator and target remains below a prescribed value. Considering detumbling operation along an arbitrary arm motion, Oki *et al.* [14] proposed a time-optimal control of a free-floating space robot to stabilize a tumbling target satellite. However, these control methods are still built on the basis of hard-docking, which will inevitably have the following constraints: position and attitude measurement, tracking and maintenance meet the high accuracy requirements.

In [15], the computed torque control method is used to design active controller to suppress the spacecraft drift caused by the impact. In order to alleviate the impact vibration resulting from objects grasping, the kinematics redundancy of a flexible redundant manipulator is employed by Xu and Yue [16]. Larouche and Zhu [17] proposed motion predictive control scheme for the autonomous capturing task. McCourt and de Silva [18] investigates the use of model-based predictive control for the capture of a multi-degrees-of-freedom object that moves in a somewhat predictable manner. Zhang *et al.* [19] put forward a scheme of pre-impact trajectory planning for minimizing the disturbance of base attitude caused by impact according to reaction null space method and particle swarm optimization algorithm. Due to the inevitable existence of model errors and operational accuracy, it is impossible to fundamentally avoid the impact and disturbance introduced by the capture process, and it is difficult to suppress the unstable vibration of the complex after the docking.

The variable stiffness technology [20] is developed to build passively compliant, robust, and dexterous robots. When interacting with the environment, the stiffness of the robot can vary according to the load change, which is very meaningful. The stiffness characteristics of variable stiffness joints plays an important role in the stability, safety and efficiency of the robot in all kinds of complex operations. They are mainly implemented in humanoid robots for many different applications. Such as joints are used in the service type robots to physically interact with humans [21]–[23]. It can also be used in humanoid robots for walking, hopping, or throwing [24]–[26]. In this paper, it is used in the manipulator to reduce the impulse brought by the impact.

This paper is organized as follows. In Section II, we introduce the dynamics of variable stiffness joint free-floating space manipulator especially at the pre-imapct and post-impact stages. In Section III, a self-learning soft-grasp control strategy based on cellular differential evolution algorithm for minimizing the angular momentum of the base is presented. Then in Section IV, according to the desired stiffness value, an adaptive backstepping sliding mode control method is applied on the adjustment motor to track the desired joint stiffness. Simulation results are discussed in Section V. Finally, Section VI gives some conclusions.

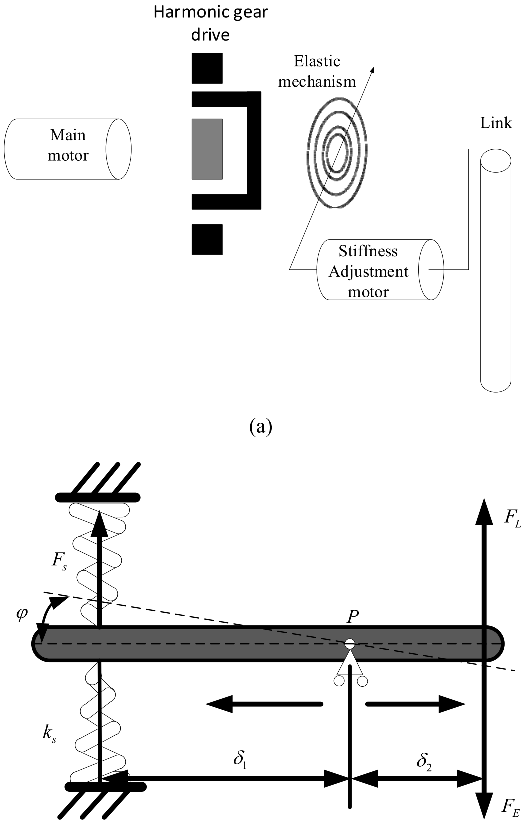

(a)

(b)

FIGURE 1. Principle of variable stiffness. (a) The variable stiffness joint. (b) The elastic mechanism schematic.

II. DYANMIC MODELING OF VARIABLE STIFFNESS JOINT FREE-FLOATING SPACE MANIPULATOR

The variable stiffness joint is shown in Fig.1(a), and its working principle is that the joint rotation is controlled by the main motor and the joint stiffness is regulated by the adjustment motor. The elastic mechanism schematic is shown in Fig.1(b), the antagonistic spring is fixed at the lever end, the external force is applied at the other end and the position is fixed.

The lever arm ratio is changed by moving the pivot position, while the pivot position is controlled by the adjustment motor. When the pivot moves towards the end of the spring, the stiffness becomes smaller, on the contrary, the stiffness becomes larger when moving towards the other end. When the space manipulator accomplishes positioning and trajectory tracking tasks, the joint stiffness is fixed to keep high stiffness. When interacting with the environment, the joint stiffness can be regulated by the adjustment motor as the load changes. This method has no special requirements for the position and attitude of the manipulator before collision.

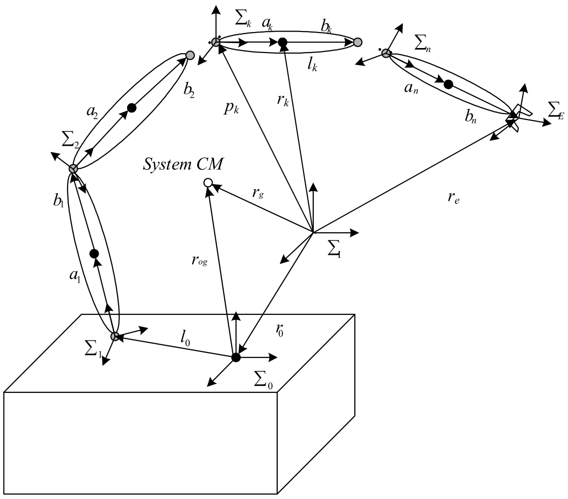

FIGURE 2. A general model of free-floating space manipulator.

We assume that the variable stiffness joint free-floating space manipulator system is composed of a free-floating base and rigid links in series, which are connected with variable stiffness joints as shown in Fig. 2, where $\sum_{\mathrm{I}}$ is the inertial frame; $\sum_i (i = 1, 2, \ldots, n)$ is the ith body frame and $\sum_0$ is the base frame. $\boldsymbol{r}_{og}$ is the vector from origin of the mass center of the base to the mass center of the system. According to the geometry of the system, the vectors of the centroid $\boldsymbol{r}_i$, the velocities $\boldsymbol{v}_i$ and angular velocities $\boldsymbol{\omega}_i$ of each body with respect to the inertial frame are represented as follows:

$$\boldsymbol{r}_i = \boldsymbol{r}_0 + \boldsymbol{l}_0 + \sum_{k=1}^{i-1} (\boldsymbol{a}_k + \boldsymbol{b}_k) + \boldsymbol{a}_i \tag{1}$$

$$\boldsymbol{v}_i = \dot{\boldsymbol{r}}_i = \boldsymbol{v}_0 + \boldsymbol{\omega}_0 \times (\boldsymbol{r}_i - \boldsymbol{r}_0) + \sum_{k=1}^{i} \left[\boldsymbol{\xi}_k \times \left(\boldsymbol{r}_k - \boldsymbol{p}_k\right)\right] \dot{\boldsymbol{q}}_k \tag{2}$$

$$\boldsymbol{\omega}_i = \boldsymbol{\omega}_0 + \sum_{k=1}^{i} \boldsymbol{\xi}_k \dot{\boldsymbol{q}}_k \tag{3}$$

where $\boldsymbol{l}_0$ is a vector pointing from center of the base to the centroid of the first joint. $\boldsymbol{r}_0$, $\boldsymbol{v}_0$, $\boldsymbol{\omega}_0$ are the position vector of the centroid of the base, the velocity and angular velocity of the base respectively. $\boldsymbol{a}_i$ is a vector pointing from center of the ith joint to the centroid of the ith body and $\boldsymbol{b}_i$ is a vector pointing from the centroid of the ith body to the center of the $(i+1)$th joint. $\boldsymbol{\xi}_i$ is the unit vector representing the rotation direction of the ith joint. $\boldsymbol{q}_i$ and $\dot{\boldsymbol{q}}_i$ are the position and motion rate of the ith joint, respectively.

Assuming the initial linear momentum and angular momentum are zero, due to the conservation of linear momentum and angular momentum, the total momentum of the system is

$$\boldsymbol{P} = \sum_{j=0}^{n} m_j \dot{\boldsymbol{r}}_j = \boldsymbol{O} \tag{4}$$

$$\boldsymbol{L} = \sum_{j=0}^{n} \left(J_j \boldsymbol{\omega}_j + \boldsymbol{r}_j \times m_j \dot{\boldsymbol{r}}_j\right) = \boldsymbol{O} \tag{5}$$

where m_j is the mass of each part; J_j is the moment of inertia of each part. Considering the angular momentum of the whole system relative to the satellite's mass center, presented by $\boldsymbol{L}_0$, then

$$\boldsymbol{L} = \boldsymbol{L}_0 + \boldsymbol{r}_0 \times \boldsymbol{P} \tag{6}$$

There is $\boldsymbol{L} = \boldsymbol{P} = \boldsymbol{O}$, so

$$\boldsymbol{L}_0 = \sum_{j=0}^{n} \left(J_j \boldsymbol{\omega}_j + \left(\boldsymbol{r}_j - \boldsymbol{r}_0\right) \times m_j \dot{\boldsymbol{r}}_j\right) = \boldsymbol{O} \tag{7}$$

Substituting (2) into (4) yields

$$\boldsymbol{P} = \left[\boldsymbol{ME} \;\; \boldsymbol{M}\tilde{\boldsymbol{r}}_{0g}^{\mathrm{T}}\right] \begin{bmatrix} \boldsymbol{v}_0 \\ \boldsymbol{\omega}_0 \end{bmatrix} + \boldsymbol{H}_{v\phi} \dot{\boldsymbol{q}} = \boldsymbol{O} \tag{8}$$

where $\boldsymbol{M}$ is the total mass of the system; $\boldsymbol{E}$ is an identity matrix; if $\boldsymbol{r}_{0g} = \begin{bmatrix} x & y & z \end{bmatrix}^{\mathrm{T}}$, then $\tilde{\boldsymbol{r}}_{0g} = \begin{bmatrix} 0 & -z & y \\ z & 0 & -x \\ -y & x & 0 \end{bmatrix}$; $\boldsymbol{H}_{v\phi}$ is the linear coupling inertial matrice.

Substituting (2) and (3) into (7) yields

$$\boldsymbol{L}_0 = \left[\boldsymbol{M}\tilde{\boldsymbol{r}}_{0g} \;\; \boldsymbol{H}_{\omega}\right] \begin{bmatrix} \boldsymbol{v}_0 \\ \boldsymbol{\omega}_0 \end{bmatrix} + \boldsymbol{H}_{\omega\phi} \dot{\boldsymbol{q}} = \boldsymbol{O} \tag{9}$$

where $\boldsymbol{H}_{\omega}$ is the angular velocity inertial matrix of the base. $\boldsymbol{H}_{\omega\phi}$ are the angular coupling inertial matrice.

The total kinetic energy of the system contains two parts: the kinetic energy of the base and rigid links and the kinetic energy of each motor rotor. Because the motor rotor mass is negligible, the rotor kinetic energy is mainly rotational kinetic energy of its own.

$$T_L = \frac{1}{2} \sum_{j=0}^{n} \left(m_j \cdot \dot{\boldsymbol{r}}_j^{\mathrm{T}} \cdot \dot{\boldsymbol{r}}_j + \frac{1}{2} \boldsymbol{\omega}_j^{\mathrm{T}} \cdot J_j \cdot \boldsymbol{\omega}_j\right) \tag{10}$$

$$T_M = \frac{1}{2} \sum_{i=1}^{n} \left(J_{di} \dot{\boldsymbol{\theta}}_{di}^2 + J_{ri} \dot{\boldsymbol{\theta}}_{ri}^2\right) \tag{11}$$

where J_{di} and J_{ri} are the moments of inertia of main motor rotor and adjustment motor rotor, respectively; $\boldsymbol{\theta}_{di}$ and $\boldsymbol{\theta}_{ri}$ are the angular vectors of the main motor and adjustment motor, respectively.

The total potential energy of the system is only elastic deformation potential energy generated by the adjustment mechanism, namely

$$V=\frac{1}{2}\sum_{i=1}^{n}\left(k_i\boldsymbol{\theta}_{si}^2\right) \tag{12}$$

where k_i represents the stiffness of the elastic mechanism. $\boldsymbol{\theta}_{si}=\left(\boldsymbol{q}_i-\boldsymbol{\theta}_{di}/N_i\right)$ is the deformation owing to the elastic mechanism. The Lagrange equation is expressed as the following form

$$\begin{bmatrix}\boldsymbol{H}_{\mathrm{b}} & \boldsymbol{H}_{\mathrm{bm}}\\ \boldsymbol{H}_{\mathrm{bm}}^{\mathrm{T}} & \boldsymbol{H}_{\mathrm{m}}\end{bmatrix}\begin{bmatrix}\ddot{\boldsymbol{x}}_{\mathrm{b}}\\ \ddot{\boldsymbol{q}}\end{bmatrix}+\begin{bmatrix}\boldsymbol{c}_{\mathrm{b}}\\ \boldsymbol{c}_{\mathrm{m}}\end{bmatrix}+\boldsymbol{K}\begin{bmatrix}\boldsymbol{O}_{6\times 1}\\ \boldsymbol{q}_i-\boldsymbol{\theta}_{di}/N_i\end{bmatrix}=\begin{bmatrix}\boldsymbol{F}_{\mathrm{b}}\\ \boldsymbol{O}_{n\times 1}\end{bmatrix}$$

$$J_{di}\ddot{\boldsymbol{\theta}}_{di}-\frac{1}{N_i}k_i\left(\boldsymbol{q}_i-\boldsymbol{\theta}_{di}/N_i\right)=\boldsymbol{\tau}_{di}$$

$$J_{ri}\ddot{\boldsymbol{\theta}}_{ri}=\boldsymbol{\tau}_{ri} \tag{13}$$

where $\boldsymbol{H}_{\mathrm{b}}$ is the inertial matrix of the base. $\boldsymbol{H}_{\mathrm{m}}$ is the manipulator inertial matrix. $\boldsymbol{H}_{\mathrm{bm}}$ is the coupling inertial matrix of base and manipulator. $\ddot{\boldsymbol{x}}_{\mathrm{b}}=\begin{bmatrix}\dot{\boldsymbol{v}}_0\\ \dot{\boldsymbol{\omega}}_0\end{bmatrix}$ denotes the base accelerations, with $\dot{\boldsymbol{v}}_0$ and $\dot{\boldsymbol{\omega}}_0$ linear and angular accelerations of the base. $\ddot{\boldsymbol{q}}=[\ddot{q}_1,\ddot{q}_2,\ldots,\ddot{q}_n]$ describes the accelerations of the joints. $\boldsymbol{c}_{\mathrm{b}}=[\,\boldsymbol{c}_{\mathrm{bv}}\ \boldsymbol{c}_{\mathrm{b}\omega}\,]^{\mathrm{T}}$ is non-linear terms of the base with $\boldsymbol{c}_{\mathrm{bv}}$ and $\boldsymbol{c}_{\mathrm{b}\omega}$ the linear and angular velocity-dependent nonlinear terms of the base. $\boldsymbol{c}_{\mathrm{m}}$ is non-linear terms of the manipulator. $\boldsymbol{K}=\begin{bmatrix}\boldsymbol{O}_{6\times 6} & \\ & k_i/N_i\end{bmatrix}$ is the stiffness matrix, with k_i the ith joint stiffness; $\boldsymbol{F}_{\mathrm{b}}=\left[\boldsymbol{f}_{\mathrm{b}},\boldsymbol{\tau}_{\mathrm{b}}\right]$ denotes the forces acting on the base by reaction wheels or jet thrusters; $\boldsymbol{\tau}_{di}$ and $\boldsymbol{\tau}_{ri}$ are respectively the driving moment of the main motor and the adjustment motor; N_i represents the reduction ratio of each joint.

Take friction and damping into account, the dynamic equation of the motor can be written as

$$J_{di}\ddot{\boldsymbol{\theta}}_{di}+\phi_{di}\dot{\boldsymbol{\theta}}_{di}-\frac{1}{N_i}k_i\left(\boldsymbol{q}_i-\boldsymbol{\theta}_{di}/N_i\right)=\boldsymbol{\tau}_{di}$$

$$J_{ri}\ddot{\boldsymbol{\theta}}_{ri}+\phi_{ri}\dot{\boldsymbol{\theta}}_{ri}=\boldsymbol{\tau}_{ri} \tag{14}$$

where ϕ_{di} and ϕ_{ri} are the damping terms of the main motor and adjustment motor, respectively.

Eliminate the base velocity acceleration term $\dot{\boldsymbol{v}}_0$ to obtain

$$\begin{bmatrix}\tilde{\boldsymbol{H}}_{\omega} & \tilde{\boldsymbol{H}}_{\omega\phi}\\ \tilde{\boldsymbol{H}}_{\omega\phi}^{\mathrm{T}} & \tilde{\boldsymbol{H}}_{\mathrm{m}}\end{bmatrix}\begin{bmatrix}\dot{\boldsymbol{\omega}}_0\\ \ddot{\boldsymbol{q}}\end{bmatrix}+\begin{bmatrix}\tilde{\boldsymbol{c}}_{b\omega}\\ \tilde{\boldsymbol{c}}_{\mathrm{m}}\end{bmatrix}+\tilde{\boldsymbol{K}}\begin{bmatrix}\boldsymbol{O}_{3\times 1}\\ \boldsymbol{q}_i-\boldsymbol{\theta}_{di}/N_i\end{bmatrix}=\begin{bmatrix}\tilde{\boldsymbol{\tau}}_{\mathrm{b}}\\ \boldsymbol{\tau}\end{bmatrix} \tag{15}$$

where

$$\tilde{\boldsymbol{H}}_{\omega}=\boldsymbol{H}_{\omega}+\boldsymbol{M}\tilde{\boldsymbol{r}}_{0g}\tilde{\boldsymbol{r}}_{0g},\quad \tilde{\boldsymbol{H}}_{\omega\phi}=\boldsymbol{H}_{\omega\phi}-\tilde{\boldsymbol{r}}_{0g}\boldsymbol{H}_{v\phi},$$
$$\tilde{\boldsymbol{H}}_{\mathrm{m}}=\boldsymbol{H}_{\mathrm{m}}-\boldsymbol{H}_{v\phi}^{\mathrm{T}}\boldsymbol{H}_{v\phi}/\boldsymbol{M},$$
$$\tilde{\boldsymbol{c}}_{b\omega}=\boldsymbol{c}_{b\omega}-\tilde{\boldsymbol{r}}_{0g}\boldsymbol{c}_{bv},\quad \tilde{\boldsymbol{c}}_{\mathrm{m}}=\boldsymbol{c}_{\mathrm{m}}-\boldsymbol{H}_{v\phi}\boldsymbol{c}_{bv}/\boldsymbol{M},$$
$$\tilde{\boldsymbol{\tau}}_{\mathrm{b}}=\boldsymbol{\tau}_{\mathrm{b}}-\tilde{\boldsymbol{r}}_{0g}\boldsymbol{f}_{\mathrm{b}},\quad \boldsymbol{\tau}=-\boldsymbol{H}_{v\phi}^{\mathrm{T}}\boldsymbol{f}_{\mathrm{b}}/\boldsymbol{M},\ \tilde{\boldsymbol{K}}=\begin{bmatrix}\boldsymbol{O}_{3\times 3} & \\ & k_i/N_i\end{bmatrix}.$$

In the pre-impact stage, the space manipulator approaches the target in the free floating state. The reaction wheel and jet thruster are closed. At the same time, the base position and attitude are not controlled. So the base driving torque is zero. The main motor works, while the adjustment motor does not work. The dynamic equation is rewritten as

$$\begin{bmatrix}\tilde{\boldsymbol{H}}_{\omega} & \tilde{\boldsymbol{H}}_{\omega\phi}\\ \tilde{\boldsymbol{H}}_{\omega\phi}^{\mathrm{T}} & \tilde{\boldsymbol{H}}_{\mathrm{m}}\end{bmatrix}\begin{bmatrix}\dot{\boldsymbol{\omega}}_0\\ \ddot{\boldsymbol{q}}\end{bmatrix}+\begin{bmatrix}\tilde{\boldsymbol{c}}_{\omega}\\ \tilde{\boldsymbol{c}}_{m}\end{bmatrix}+\tilde{\boldsymbol{K}}\begin{bmatrix}\boldsymbol{O}_{3\times 1}\\ \boldsymbol{q}_i-\boldsymbol{\theta}_{di}/N_i\end{bmatrix}=\begin{bmatrix}-\tilde{\boldsymbol{r}}_{0g}\boldsymbol{f}_{\mathrm{b}}\\ -\dfrac{\boldsymbol{H}_{v\phi}^{\mathrm{T}}}{\boldsymbol{M}}\boldsymbol{f}_{\mathrm{b}}\end{bmatrix}$$

$$J_{di}\ddot{\boldsymbol{\theta}}_{di}+\phi_{di}\dot{\boldsymbol{\theta}}_{di}-\frac{1}{N_i}k_i\left(\boldsymbol{q}_i-\boldsymbol{\theta}_{di}/N_i\right)=\boldsymbol{\tau}_{di} \tag{16}$$

In the post-impact stage, the main motor brakes for reducing the system stiffness and buffering the impact momentum, and the adjustment motor works to regulate the joint stiffness. The dynamic equation is rewritten as

$$\begin{bmatrix}\tilde{\boldsymbol{H}}_{\omega} & \tilde{\boldsymbol{H}}_{\omega\phi}\\ \tilde{\boldsymbol{H}}_{\omega\phi}^{\mathrm{T}} & \tilde{\boldsymbol{H}}_{\phi}\end{bmatrix}\begin{bmatrix}\dot{\boldsymbol{\omega}}_0\\ \ddot{\boldsymbol{q}}\end{bmatrix}+\begin{bmatrix}\tilde{\boldsymbol{c}}_{\omega}\\ \tilde{\boldsymbol{c}}_{\mathrm{m}}\end{bmatrix}+\tilde{\boldsymbol{K}}'\begin{bmatrix}\boldsymbol{O}_{3\times 1}\\ \boldsymbol{q}_i-\boldsymbol{\theta}_{Di}/N_i\end{bmatrix}$$
$$=\begin{bmatrix}-\tilde{\boldsymbol{r}}_{0g}\boldsymbol{f}_{\mathrm{b}}\\ -\dfrac{\boldsymbol{H}_{v\phi}^{\mathrm{T}}}{\boldsymbol{M}}\boldsymbol{f}_{\mathrm{b}}\end{bmatrix}+\begin{bmatrix}\tilde{\boldsymbol{J}}_{b\omega}^{\mathrm{T}}\\ \tilde{\boldsymbol{J}}_{\mathrm{m}}^{\mathrm{T}}\end{bmatrix}\boldsymbol{F}_e$$
$$J_{ri}\ddot{\boldsymbol{\theta}}_{ri}+\phi_{ri}\dot{\boldsymbol{\theta}}_{ri}$$
$$=\boldsymbol{\tau}_{ri}-\boldsymbol{\tau}_{Ri} \tag{17}$$

where $\boldsymbol{\theta}_{Di}$ is the terminate angle of the main motor before contact. $\boldsymbol{F}_e$ is the external force applied on the end-effector. $\tilde{\boldsymbol{J}}_{b\omega}^{\mathrm{T}}=\boldsymbol{J}_{b\omega}^{\mathrm{T}}-\tilde{\boldsymbol{r}}_{0g}\boldsymbol{J}_{bv}^{\mathrm{T}}$, $\tilde{\boldsymbol{J}}_{\mathrm{m}}^{\mathrm{T}}=\boldsymbol{J}_{\mathrm{m}}^{\mathrm{T}}-\boldsymbol{H}_{v\phi}\boldsymbol{J}_{bv}^{\mathrm{T}}/\boldsymbol{M}$. $\boldsymbol{J}_{bv}$ and $\boldsymbol{J}_{b\omega}$ are the linear and angular velocity Jacobian matrices of the base, respectively. $\boldsymbol{J}_{\mathrm{m}}$ is the Jacobian matrix of the manipulator. $\boldsymbol{\tau}_{Ri}$ is the resistance torque on the adjustment motor. $\tilde{\boldsymbol{K}}'=\begin{bmatrix}\boldsymbol{O}_{3\times 3} & \\ & \tilde{k}_i\end{bmatrix}$ is the stiffness matrix after impact, with $\tilde{k}_i$ the ith variable joint stiffness.

Remark 1: Eq.(16) and Eq.(17) show the pre-impact and post-impact stage dynamics characteristics, respectively. The joint stiffness are a constant value in Eq.(16) and a variable value in Eq.(17).

III. SELF-LEARNING SOFT-GRASP CONTROL FOR MINIMIZING BASE ANGULAR MOMENTUM

In the post-impact stage, the main problem is how to reduce the angular momentum introduced by the impulse. For a free-floating space manipulator, the base and the manipulator is coupled. As a result, it is multi-objective optimization for minimizing the base angular momentum. At present, self-learning feedback control based on neural network is an effective method to solve the problem of complex system optimization [27]–[29]. In this paper, a novel hybrid on-line algorithm cellular differential evolution combined opposition-based learning with orthogonal crossover (CDEOLOC) is used to solve the desired joint stiffness to realize the self-learning soft-grasp control strategy of free-floating space manipulator.

A. CDEOLOC

Differential Evolution algorithm (DE) originally developed by Storn and Price [30] is an evolutionary computation technique mainly used for solving global optimization problems. The process of solving DE is basically the same as genetic algorithms, including mutation, crossover and selection. An important symbol different from genetic algorithm is DE through the differential strategy to achieve individual variation, which can keep diversity in population to explore the local search. The main structure of DE is given as follows:

Generate initial population randomly:

$$\boldsymbol{X}_i^G = [x_{i,1}^G, x_{i,2}^G, \cdots, x_{i,j}^G],\ \ j=1,2,\cdots,d,\ \ i=1,2,\cdots,NP \tag{18}$$

$$x_{i,j}^G = a_j + rand \cdot (b_j - a_j) \tag{19}$$

where $G = 0, 1, 2, \cdots, G_{\max}$ represents the evolution generation and $G_{\max}$ is the maximum generation. NP is the number of population and d is the dimension of each population. $\boldsymbol{X}_i^G$ is ith individual of G generation with $x_{i,j}^G$ representing jth dimension of ith individual of G generation. b_j and a_j are upper and lower bounds of individual $x_{i,j}^G$, respectively. $rand$ is uniformly distributed random number in [0,1].

The standard mutation operation of DE is usually to generate a new individual by selecting two different individuals from the parent population randomly and adding their difference vector to another parent individual as in the form:

$$\boldsymbol{V}_i^G = \boldsymbol{X}_{r1}^G + F \cdot (\boldsymbol{X}_{r2}^G - \boldsymbol{X}_{r3}^G) \tag{20}$$

where $i \neq r1 \neq r2 \neq r3$, $r1$, $r2$ and $r3$ are three distinct random integers in $[1, NP]$. F is the scale factor to control the search step.

In order to ensure the validity of the generated mutation individual, it is necessary to judge whether the individual dimensions of the generated test individuals are in the search space of the problem. The individuals who satisfy the condition are retained, and the individuals who are not satisfied with the condition are generated by the initialization of the population.

$$V_{i,j}^G = \begin{cases} a_j + rand \cdot \left(b_j - a_j\right) & \text{if } V_{i,j}^G < a_j \text{ or } V_{i,j}^G > b_j \\ V_{i,j}^G & \text{otherwise} \end{cases} \tag{21}$$

The basic idea of crossover operation is that mutation individual and the original individual are chosen to cross to increase the diversity of the population. In general, the cross pattern includes exponential cross and binomial cross. Usually we choose the binomial cross pattern as following

$$u_{i,j}^G = \begin{cases} V_{i,j}^G & \text{if (rand} \leq C_r\text{)or } j = j_{rand} \\ x_{i,j}^G & \text{otherwise} \end{cases} \tag{22}$$

where j_{rand} is uniformly distributed random number in $[1, d]$. C_r is crossover factor. The cross pattern can ensure that at least one dimension of the test individual $\boldsymbol{U}_i^G$ is derived from the mutation individual $\boldsymbol{V}_i^G$, thus avoiding the same as the parent individuals $\boldsymbol{X}_i^G$.

The selection operation determines the evolutionary direction of the entire population. After the generation of the offspring by mutation and crossover, the offspring in the new population is compared with the corresponding parent by a one-to-one greedy choice. The choice of the winner to be saved to the next generation and the selection process is as follows

$$\boldsymbol{X}_i^{G+1} = \begin{cases} \boldsymbol{U}_i^G, & \text{if} f\left(\boldsymbol{U}_i^G\right) \leq f\left(\boldsymbol{X}_i^G\right) \\ \boldsymbol{X}_i^G, & \text{otherwise} \end{cases} \tag{23}$$

As with genetic algorithms, DE algorithm has a strong global convergence ability and robustness. Besides, DE algorithm has less parameter and only two main parameters need to be adjusted. While the same as other evolution algorithms, DE is easy to get into local optimum and get premature convergence optimal control problems.

Cellular automata has the characteristics of parallel evolution, which can be used to balance the exploration ability and development ability of the differential evolution algorithm. The cellular differential evolution (CDE) is proposed by Nasimul and Hitoshi [31].

The basic components of cellular automata are cellular, cellular space, neighbor and rule four parts. $A = (L_u, S, N, f)$, where A represents a CA system. L_u is cellular space with u a positive integer. S is a finite and discrete set of states of cell. N is a collection of cells in all domains, including a space vector of h different cellular states, expressed as $N = (s_1, s_2, \ldots, s_h)$, where $s_i \in S$, $i \in \{1, 2, \ldots, h\}$. f is local mapping or local rule. The common neighborhood structure has four kinds, we utilize the C9 neighborhood structure (see Fig. 3).

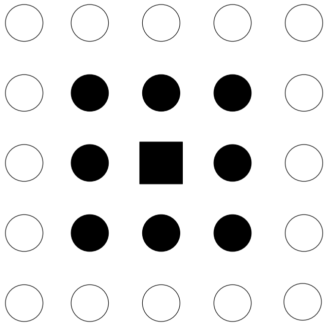

FIGURE 3. C9 neighborhood structure.

Basic evolution rule is as following,

$$\text{if } S_T = 1, \quad \text{then } S_{T+1} = \begin{cases} 1, & S \in S1 \\ 0, & S \notin S1 \end{cases} \tag{24}$$

$$\text{if } S_T = 0, \quad \text{then } S_{T+1} = \begin{cases} 1, & S \in S2 \\ 0, & S \notin S2 \end{cases} \tag{25}$$

where S_T and S_{T+1} are the cellular states after the evolution T and $(T + 1)$ steps, with *S1* expressing the number of live neighbors required to maintain live cells' states and $S2$ expressing the number of live neighbors required to resurrect the dead cells. C9 neighborhood structure has the best performance and adopts following three rules to simulate the stability, cycle and complexity of three states of life system, respectively.

$$\text{Rule1}\begin{cases}\text{if } S_T=1, & \text{then } S_{T+1}=\begin{cases}1, & S=2,3\\0, & S\neq 2,3\end{cases}\\ \text{if } S_T=0, & \text{then } S_{T+1}=\begin{cases}1, & S=3\\0, & S\neq 3\end{cases}\end{cases}\tag{26}$$

$$\text{Rule2}\begin{cases}\text{if } S_T=1, & \text{then } S_{T+1}=\begin{cases}1, & S=1,2,3,4\\0, & S\neq 1,2,3,4\end{cases}\\ \text{if } S_T=0, & \text{then } S_{T+1}=\begin{cases}1, & S=4,5,6,7\\0, & S\neq 4,5,6,7\end{cases}\end{cases}\tag{27}$$

$$\text{Rule3}\begin{cases}\text{if } S_T=1, & \text{then } S_{T+1}=\begin{cases}1, & S=2,4,6,8\\0, & S\neq 2,4,6,8\end{cases}\\ \text{if } S_T=0, & \text{then } S_{T+1}=\begin{cases}1, & S=1,3,5,7\\0, & S\neq 1,3,5,7\end{cases}\end{cases}\tag{28}$$

When without prior knowledge, using opposition-based learning to initialize the population can improve the quality of the initial solution of evolution algorithm and make the search process faster.

Generate initial population randomly as Eq.(19). Then solve the opposite individuals (see Eq.(29)) of the initial population individuals and add them into the initial population. Finally, the individual with high adaptability is chosen to form a new initial population.

$$x_{i,j}^{G'}=a_j+b_j-x_{i,j}^{G}\tag{29}$$

The purpose of crossover operation is that next generation chromosomes inherit the good genes of the parent chromosomes. However, the classical differential evolution algorithm uses a bit of crossover operation, so the above-mentioned purpose can not be achieved in most cases. The use of multiple-point crossover operation can avoid this problem. However, the multiple-point crossover operation has many possibilities because of the cross combination, so the combination will show explosive growth.

Orthogonal design is to arrange the multi-factor experiment rationally by using the prepared orthogonal table, in order to obtain the satisfactory result through a small number of experiment times. Compared with the binomial crossover algorithm, orthogonal crossover operator provides the repeated test of high-dimensional and multiple elements, so that the proposed CDEOLOC is easier to find the optimal offspring and keep the population diversity.

The orthogonal table used in DE algorithm of this paper is presented as $L_Q\left(2^d\right)$ [32], where Q is the total number of experiments and d is also the dimension of each population. The number 2 indicates that all of factors has two levels, namely represents whether the certain dimension of test individual is selected from the mutation individual or the original individual, respectively.

The CDEOLOC steps are as follows:

a) Initialization

ai) Set the population size NP and the generation $G=0$, initialize shrink factor F, and determine algorithm termination conditions.

aii) Generate $NP=np\times np$ initial individuals $x_{i,j}^{G}$ and their opposite individuals $x_{i,j}^{G'}$ in the search space randomly. Evaluate all individuals to obtain $NP=np\times np$ better individuals $\tilde{x}_{i,j}^{G}$ according to fitness function.

aiii) In cellular automata, each cell state is randomly initialized, corresponding to each individual's state of existence.

aiiii) Generate the orthogonal crossover table.

b) Live individuals evolve by iteration. If there is no live individual, skip to step c).

bi) Individual chooses candidates from neighbor cells to mutate.

bii) Adjust the shrink factor F adaptively then perform the mutation and deal with the boundary conditions.

biii) Perform crossover operations following orthogonal design.

biiii) Evaluate individuals according to fitness function and renew the next population.

c) Cellular automata evolves in accordance with evolutionary rule to determine the new generation of cells' existence conditions and $G=G+1$.

d) Determine whether the termination condition is satisfied. If true, the iteration is terminated and the optimal individual at this moment is output. Otherwise, continue to the b) step.

The steps for implementing CDEOLOC are simply shown in Fig. 4

B. OBJECTIVE FUNCTION AND SELF-LEARNING SOFT-GRASP CONTROL FLOW

For the manipulator structure mentioned in the second section, after the contact, the impact force will make the system momentum alter. Meanwhile, the base momentum will occur large change. The control objective of the flexible arm is to weak the base angular velocity. But for free-floating space manipulator, the base is coupled with the manipulator and the disturbance of the joints will also influence the base. So, we set up the objective function as follow

$$F=\min\left(\eta_0\left\|\boldsymbol{\omega}_0\right\|+\eta_1\left\|\dot{\boldsymbol{q}}_1\right\|+\eta_2\left\|\dot{\boldsymbol{q}}_2\right\|+\ldots+\eta_n\left\|\dot{\boldsymbol{q}}_n\right\|\right)\tag{30}$$

where $\eta_0, \eta_1, \eta_2 \ldots \eta_n$ are weighting coefficients which satisfy $\eta_0+\eta_1+\eta_2\ldots+\eta_n=1$. Owing to the coupling between the base and the manipulator, the angular momentum will all be transferred to the base. So the objective function can not reach zero. The final weights are determined by the test.

In order to minimize the base angular momentum, we present the control strategy flow as follows:

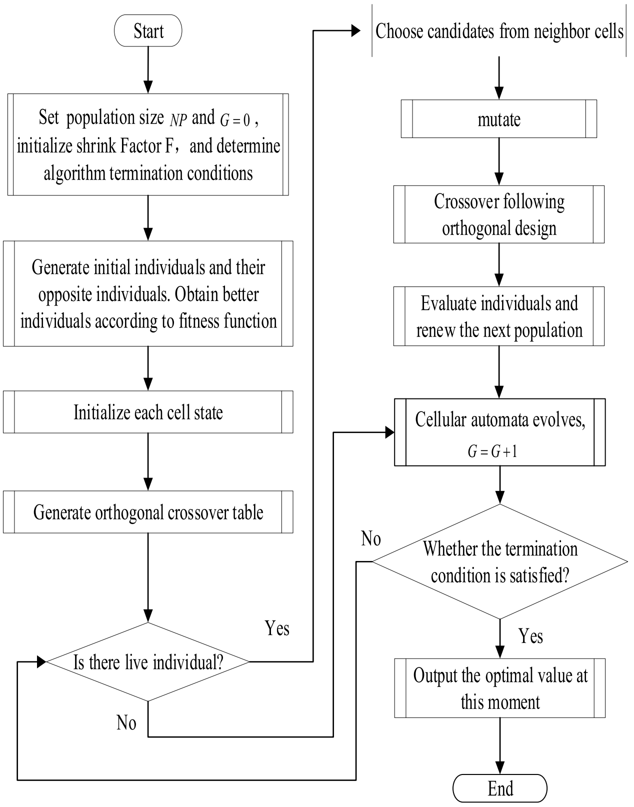
Start
Set population size NP and $G=0$, initialize shrink Factor F, and determine algorithm termination conditions
Generate initial individuals and their opposite individuals. Obtain better individuals according to fitness function
Initialize each cell state
Generate orthogonal crossover table
Is there live individual?
Yes
No
Choose candidates from neighbor cells
mutate
Crossover following orthogonal design
Evaluate individuals and renew the next population
Cellular automata evolves, $G=G+1$
Whether the termination condition is satisfied?
No
Yes
Output the optimal value at this moment
End

FIGURE 4. **CDEOLOC steps.**

Step 1) After the contact, the motion sensor detects the rotation angles and angular velocities $\boldsymbol{x}(t)$ of each joint and base at time t.

Step 2) Substitute $\boldsymbol{x}(t)$ and the stiffness value after crossover into the fitness function of CDEOLOC which calls Lagrange dynamics equation, then through the CDEOLOC to calculate the desired joint stiffness values at time t.

Step3) Through adjusting the stiffness adjustment motor, output desired joint stiffness value at time t. The sensor detects the rotation angles and angular velocities $\boldsymbol{x}(t+1)$ of the joint and the base at time $t+1$.

Step 4) Repeat step 2) and calculate the desired joint stiffness value at time $t+1$. Keep repeating until the terminate time.

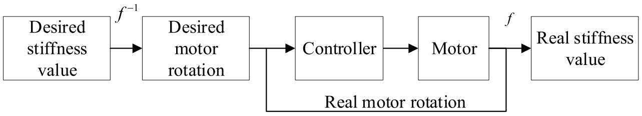

FIGURE 5. **Real motor rotation solving process.**

IV. SOLVING THE REAL JOINT STIFFNESS

Due to the stiffness of joint has a non-linear function with the angle of the adjustment motor, the stiffness of joint can not be directly controlled. If the desired stiffness value is known, the real stiffness value can be obtained through the motor rotation control. The control structure is shown in Fig.5.

A. ADAPTIVE BACKSTEPPING SLIDING MODE CONTROL ALGORITHM

The dynamic equation of adjustment motor is defined as the second equation in Eq. (17). The resistance torque on the adjustment motor τ_R is expressed as

$$\tau_R = f\left(\theta_r, \theta_s\right) \tag{31}$$

Considering that the change of θ_s related to the load and characteristic of the elastic mechanism has uncertainty, it is regarded as external interference signal. In addition, the variation of the external load will cause the change of the motor inertia and other parameters in the system. Thus, the dynamic equation of adjustment motor can be changed into

$$\hat{J}_r\ddot{\theta}_r + \hat{\phi}_r\dot{\theta}_r = \tau + \rho\left(\theta_r, \dot{\theta}_r, \ddot{\theta}_r\right) \tag{32}$$

where $\hat{J}_r$ and $\hat{\phi}_r$ are the estimate values of J_r and ϕ_r, respectively. So

$$\begin{aligned} J_r &= \hat{J}_r + \Delta J_r \\ \phi_r &= \hat{\phi}_r + \Delta\phi_r \end{aligned} \tag{33}$$

ΔJ_r and $\Delta\phi_r$ are uncertainty of J_r and ϕ_r, respectively. The overall uncertainty of the system $\rho\left(\theta_r, \dot{\theta}_r, \ddot{\theta}_r\right)$ is expressed as

$$\rho\left(\theta_r, \dot{\theta}_r, \ddot{\theta}_r\right) = -\Delta J_r\ddot{\theta}_r - \Delta\phi_r\dot{\theta}_r - \tau_R \tag{34}$$

Assuming that $\rho\left(\theta_r, \dot{\theta}_r, \ddot{\theta}_r\right)$ satisfies the following condition

$$\left|\rho\left(\theta_r, \dot{\theta}_r, \ddot{\theta}_r\right)\right| \leq \rho^* \tag{35}$$

Eq.(32) can be rewritten as

$$\ddot{\theta}_r = \hat{J}_r^{-1}\left(-\hat{\phi}_r^{-1}\dot{\theta}_r + \tau + \rho\left(\theta_r, \dot{\theta}_r, \ddot{\theta}_r\right)\right) \tag{36}$$

The dynamic equation of the adjustment motor is a second-order nonlinear system, so we utilize the backstepping design method. The basic idea of the backstepping design method is to decompose the complex nonlinear system into subsystems not exceeding the order of the system, and then design the Lyapunov function and the intermediate virtual control variable for each subsystem. Keep "back" until the whole control law is designed. Apart from this, designing the intermediate virtual control variable through the sliding mode thought can simplify the system. Because of the external disturbance and uncertain system parameters, it is difficult to obtain the exact upper bound ρ^* of $\rho\left(\theta_r, \dot{\theta}_r, \ddot{\theta}_r\right)$ actually. Adaptive control is adopted to realize the adaptive estimation of upper bound ρ^* of $\rho\left(\theta_r, \dot{\theta}_r, \ddot{\theta}_r\right)$.

Therefore, an adaptive backstepping sliding mode controller is designed by combining the backstepping design, sliding mode control and adaptive control. Assume that the motor desired trajectory is θ_{rd}. $\dot{\theta}_{rd}$ and $\ddot{\theta}_{rd}$ are corresponding desired velocity and acceleration. The position and velocity tracking error are defined as

$$e = \theta_r - \theta_{rd} \tag{37}$$

$$\dot{e} = \dot{\theta}_r - \dot{\theta}_{rd} \tag{38}$$

The Lyapunov function candidate is defined as

$$V_1 = \frac{1}{2}e^2 \tag{39}$$

Furthermore, define intermediate virtual control variable η as

$$\eta = \dot{e} + c_1 e = \dot{\theta}_r - \dot{\theta}_{rd} + c_1 e \tag{40}$$

where c_1 is a positive constant.

Differentiating (39) and utilizing (40) yields

$$\dot{V}_1 = e\dot{e} = e\left(\eta - c_1 e\right) = e\eta - c_1 e^2 \tag{41}$$

where if $\eta = 0$, $\dot{V}_1 \leq 0$.

Define the sliding surface as

$$\sigma = k_1 e + \eta \tag{42}$$

where k_1 is a positive constant. Then the Lyapunov function candidate is defined as

$$V_2 = V_1 + \frac{1}{2}\sigma^2 + \frac{1}{2\lambda}\rho^2 \tag{43}$$

where λ is a positive constant, $\rho = \rho^* - \hat{\rho}$, $\hat{\rho}$ is the upper estimated value of total uncertainty ρ.

Differentiating (43), setting $B = \sigma\hat{J}_r^{-1}$ and $W = |B|$, combining (36) and (42) we have

$$\begin{aligned}
\dot{V}_2 &= \dot{V}_1 + \sigma\dot{\sigma} - \frac{1}{\lambda}\rho\dot{\rho} \\
&= e\eta - c_1 e^2 + \sigma\left(k_1\dot{e} - \hat{J}_r^{-1}\hat{\phi}_r\theta_r\right. \\
&\qquad \left. + \hat{J}_r^{-1}\tau + \hat{J}_r^{-1}\rho - \ddot{\theta}_{rd} + c_1\dot{e}\right) - \frac{1}{\lambda}\rho\dot{\rho} \\
&\leq e\eta - c_1 e^2 + \sigma\left(k_1\dot{e} - \hat{J}_r^{-1}\hat{\phi}_r\theta_r\right. \\
&\qquad \left. + \hat{J}_r^{-1}\tau + \hat{J}_r^{-1}\rho - \ddot{\theta}_{rd} + c_1\dot{e}\right) + W\rho^* - \frac{1}{\lambda}\rho\dot{\rho} \\
&= e\eta - c_1 e^2 + \sigma\left[k_1\left(\eta - c_1 e\right) - \hat{J}_r^{-1}\hat{\phi}_r\left(\eta + \dot{\theta}_{rd} - c_1 e\right)\right. \\
&\qquad \left. + \hat{J}_r^{-1}\tau - \ddot{\theta}_{rd} + c_1\dot{e}\right] + W\hat{\rho} - \frac{1}{\lambda}\rho\left(\dot{\hat{\rho}} - \lambda W\right)
\end{aligned} \tag{44}$$

The adaptive backstepping sliding mode controller is designed as

$$\begin{aligned}
\tau = \hat{J}_r\Big[&-k_1\left(\eta - c_1 e\right) + \hat{J}_r^{-1}\hat{\phi}_r\left(\eta + \dot{\theta}_{rd} - c_1 e\right) \\
&+ \ddot{\theta}_{rd} - c_1\dot{e} - \beta\sigma\Big] - \hat{\rho}sgn\left(\sigma\right)
\end{aligned} \tag{45}$$

where β is a positive constant. Simultaneously, the adaptive control law is defined as

$$\dot{\hat{\rho}} = \lambda W \tag{46}$$

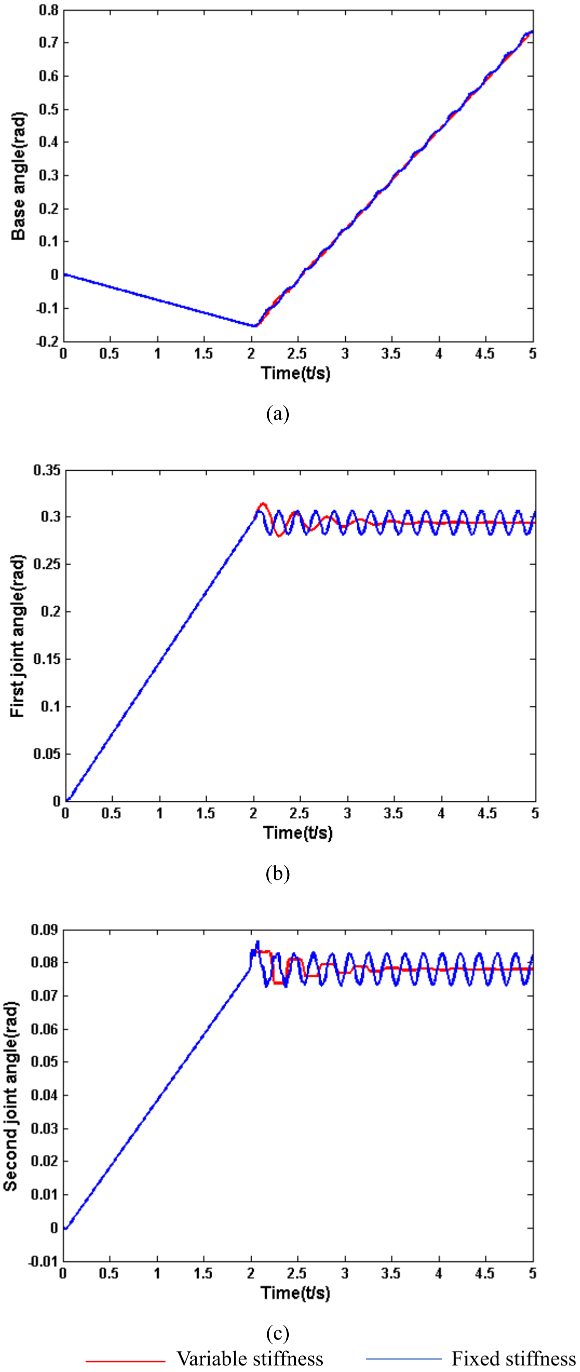

(a)

(b)

(c)

FIGURE 6. Base and joints angle. (a) The base angle. (b) The first joint angle. (c) The second joint angle.

Substituting (45) and (46) into (44) yields

$$\dot{V}_2 \leq e\eta - c_1 e^2 - \beta\sigma^2 \tag{47}$$

Set

$$\boldsymbol{Y} = \begin{bmatrix} c_1 + \beta k_1^2 & \beta k_1 - \dfrac{1}{2} \\ \beta k_1 - \dfrac{1}{2} & \beta \end{bmatrix} \tag{48}$$

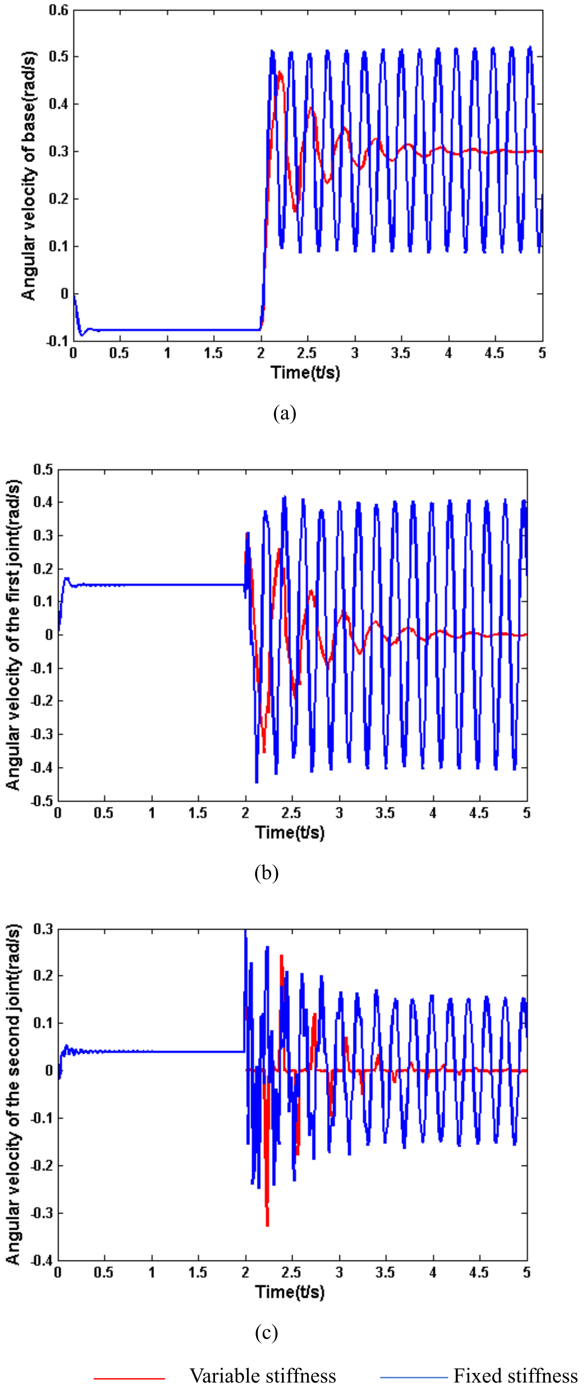

(a)

(b)

(c)

FIGURE 7. Base and joints angular velocities. (a) The base angular velocity. (b) The first joint angular velocity. (c) The second joint angular velocity.

Owing to

$$\begin{bmatrix} e & \eta \end{bmatrix} \begin{bmatrix} c_1 + \beta k_1^2 & \beta k_1 - \dfrac{1}{2} \\ \beta k_1 - \dfrac{1}{2} & \beta \end{bmatrix} \begin{bmatrix} e \\ \eta \end{bmatrix}$$
$$= c_1 e^2 + \beta k_1^2 e^2 + 2\eta\beta k_1 e + \beta\eta^2 - \eta e$$
$$= c_1 e^2 + \beta\sigma^2 - \eta e \tag{49}$$

TABLE 1. Key parameters.

Description	Symbol	Value	Unit
Base mass	m_0	40	kg
First joint mass	m_1	4	kg
Second joint mass	m_2	3	kg
Base inertia	J_0	6.667	$\mathrm{kg \cdot m^2}$
First joint inertia	J_1	0.33	$\mathrm{kg \cdot m^2}$
Second joint inertia	J_2	0.25	$\mathrm{kg \cdot m^2}$
First joint and second joint stiffness	k_1 、 k_2	3000	N · m/rad
Vector from center of the base to the centroid of the first joint	l_0	0.5	m
Vector from center of the first joint to the centroid of the first body and vector from center of the second joint to the centroid of the second body	a_1 、 a_2	0.5	m
Vector from the centroid of the first body to the center of the second joint and vector from the centroid of the second body to the center of the end-effector	b_1 、 b_2	0.5	m
First main motor drive torque	τ_{d1}	0.15	N
Second main motor drive torque	τ_{d2}	0.04	N
First main motor inertia	J_{d1}	1.06×10^4	$\mathrm{kg \cdot m^2}$
Second main motor inertia	J_{d2}	1.73×10^4	$\mathrm{kg \cdot m^2}$
First main motor and second main motor damping	ϕ_{d1} 、 ϕ_{d2}	0.01	N · ms/rad
Max iteration	G_m	100	
Population size	NP	15	

set $\boldsymbol{S} = [e\ \eta]^{\mathrm{T}}$. Then Eq. (47) can be written as

$$\dot{V}_2 \leq -\boldsymbol{s}^{\mathrm{T}} \boldsymbol{Y} \boldsymbol{s} \tag{50}$$

Remark 2: Select proper positive constant c_1, k_1 and β to ensure that $\boldsymbol{Y}$ is a symmetric positive definite matrix. Hence $\dot{V}_2 \leq 0$. The design of the adaptive backstepping sliding mode controller makes the system satisfy the Lyapunov stability.

V. SIMULATION

A. CDEOLOC CONTROL FOR MINIMIZING BASE ANGULAR MOMENTUM

In order to verify the validity of the method in this paper, use the model of a planar two-DOF free-floating space robot described in the second section as an example of numerical simulation. The system parameters and algorithm parameters are shown in Table 1.

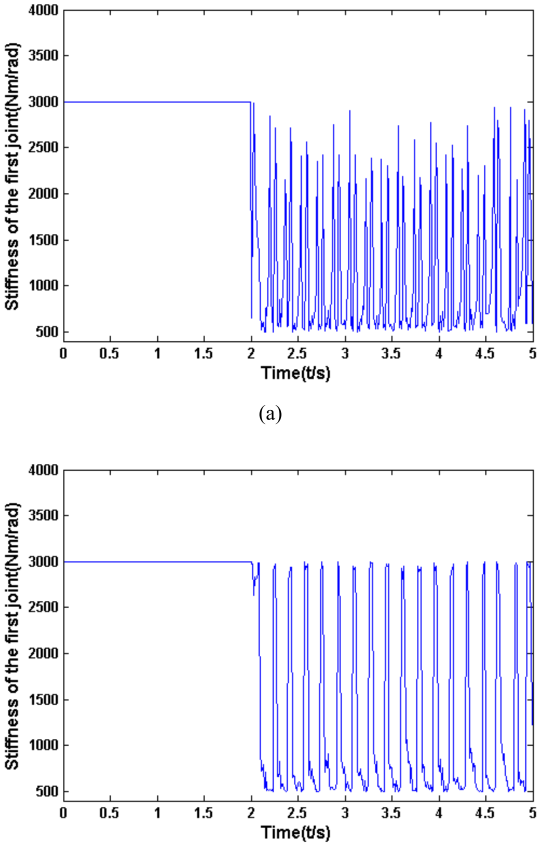

(a)

(b)

FIGURE 8. Stiffness variation of the joints. (a) Stiffness variation of the first joint. (b) Stiffness variation of the second joint.

Besides, the manipulator starts from $v_0 = 0$rad, $\omega_0 = 0$rad/s, $q = [0, 0]$ rad, $\dot{q} = [0, 0]$rad/s. Stiffness adjustment range is [500, 3000]Nm/rad and impact force is $F = [30, 40]$N. Simulation time is 5s and the simulation step size is 0.01s. The impact occurs at t = 2s and lasts for 0.1s.

Fig. 6 shows that the angles of joints are approaching the angles before the impact gradually after two seconds under optimization control. The base angle still changes over time under the control. From Fig. 7, we can see that after impact, both of the base and the joints angular velocities occur obvious vibration and they are significantly weakened when using CDEOLOC control strategy. Fig. 7(a) shows that the amplitude of the base angular velocity is weakened by 40 percent and Fig. 7(b) and Fig. 7(c) shows that the joint angular velocity is weakened to zero. Though the base does not stop rotating, the instantaneous impact brought to it is decreased and the residual vibration is obviously suppressed, which means the optimization is valid. Fig. 8 proves that the changes of joint stiffness are within the adjustment range.

B. ADAPTIVE BACKSTEPPING SLIDING MODE CONTROL

In the simulation process, the involved parameters are $J_r = 0.106\text{kgm}^2$, $\phi_r = 0.5$Nms/rad, and $\hat{J}_r = 0.8J_r$, $\hat{\phi}_r = 0.8\phi_r$. The corresponding parameters of backstepping sliding mode controller are selected as $c_1 = 3, k_1 = 2, \beta = 3$, and $\lambda = 0.5$.

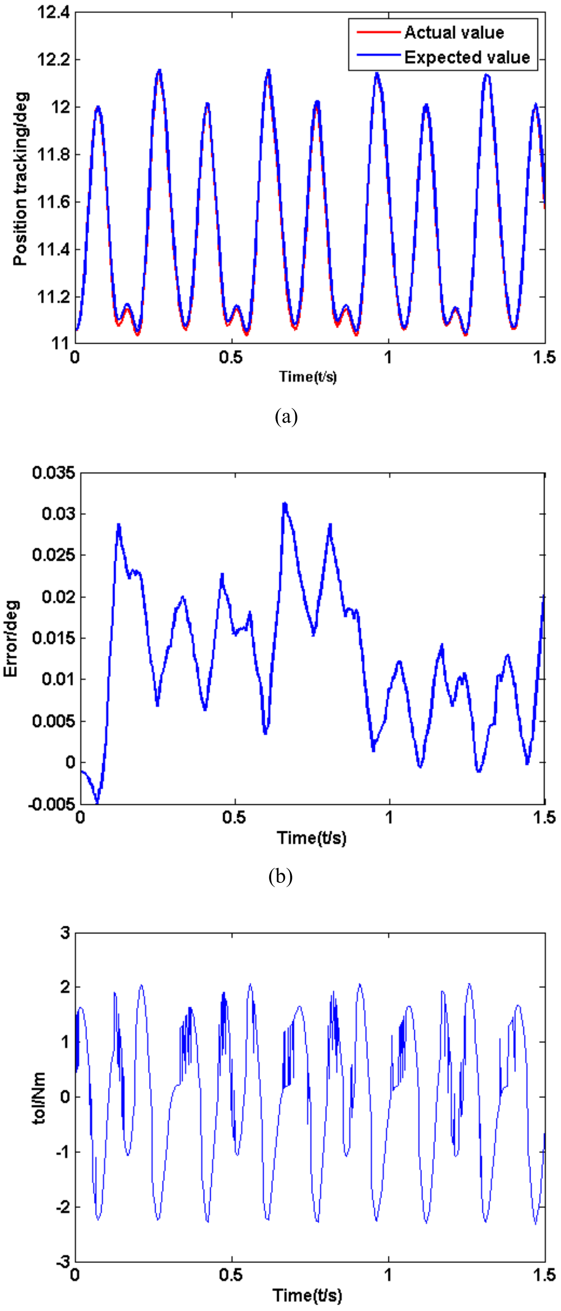

(a)

(b)

(c)

FIGURE 9. Adaptive backstepping sliding mode control results. (a) Position tracking of the adjustment motor. (b) Position tracking error of the adjustment motor. (c) Output torque of the controller.

From the Fig.9, one can see that the adjustment motor can accurately track the desired trajectory, and both the tracking error and the output torque are bounded. The adaptive backstepping sliding mode control scheme designed in this paper can effectively eliminate the influence of the system inertia parameter uncertainty and external disturbance on the motor system.

VI. CONCLUSIONS

With the development of the space robotics, the free-floating space manipulator plays an important role in space capturing operation. But the base attitude is easily disturbed by impact due to the coupling between the base and the manipulator. This paper summarizes the main methods to reduce the base attitude angular momentum and proposes a new strategy on the basis of variable stiffness method. When the space manipulator suffered from external impact, the stiffness of joint can be regulated to reduce the impact and guarantee the angular momentum does not exceed the limit, which is clearly verified with the desired joint stiffness control method based on CDEOLOC. The simulation results show that improving the flexibility of the space manipulator by changing the joint stiffness can buffer the impulse introduced by collision effectively.

ACKNOWLEDGMENT

The authors would like to thank anonymous reviewers for their valuable comments to improve the quality of this paper.

REFERENCES

[1] A. Flores-Abad, O. Ma, K. Pham, and S. Ulrich, "A review of space robotics technologies for on-orbit servicing," *Prog. Aerosp. Sci.*, vol. 68, pp. 1–26, Jul. 2014.

[2] J. Wu, S. Shi, H. Liu, and H. Cai, "Spacecraft attitude disturbance optimization of space robot in target capturing process," *Robot*, vol. 33, no. 1, pp. 16–21, 2011.

[3] K. Yoshida, N. Sashida, R. Kurazume, and Y. Umetani, "Modeling of collision dynamics for space free-floating links with extended generalized inertia tensor," in *Proc. IEEE Int. Conf. Robot. Autom.*, May 1992, pp. 899–904.

[4] K. Yoshida and N. Sashida, "Modeling of Impact Dynamics and Impulse Minimization for Space Robots," in *Proc. IEEE/RSJ Int. Conf. Intell. Robot. Syst.*, Yokohama, Japan, Jul. 1993, pp. 2064–2069.

[5] L.-B. Wee and M. W. Walker, "On the dynamics of contact between space robots and configuration control for impact minimization," *IEEE Trans. Robot. Autom.*, vol. 9, no. 5, pp. 581–591, Oct. 1993.

[6] D. N. Nenchev, K. Yoshida, P. Vichitkulsawat, and M. Uchiyama, "Reaction null-space control of flexible structure mounted manipulator systems," *IEEE Trans. Robot. Autom.*, vol. 15, no. 6, pp. 1011–1023, Dec. 1999.

[7] D. N. Nenchev and K. Yoshida, "Impact analysis and post-impact motion control issues of a free-floating Space robot subject to a force impulse," *IEEE Trans. Robot. Autom.*, vol. 15, no. 3, pp. 548–557, Jun. 1999.

[8] K. Yoshida and H. Nakanishi, "Impedance matching in capturing a satellite by a space robot," in *Proc. Int. Conf. Intell. Robot. Syst.*, Las Vegas, NV, USA, Oct. 2003, pp. 27–31.

[9] P. C. Cong and X. Zhang, "Preimpact configuration analysis of a dual-arm space manipulator with a prismatic joint for capturing an object," *Robotica*, vol. 31, no. 6, pp. 853–860, 2013.

[10] D. N. Dimitrov and K. Yoshida, "Utilization of the bias momentum approach for capturing a tumbling satellite," in *Proc. IEEE/RSJ Int. Conf. Intell. Robot. Syst.*, Sep./Oct. 2004, pp. 3333–3338.

[11] D. N. Dimitrov and K. Yoshida, "Momentum distribution in a space manipulator for facilitating the post-impact control," in *Proc. IEEE/RSJ Int. Conf. Intell. Robot. Syst.*, Sep./Oct. 2004, pp. 3345–3350.

[12] H. Shui, X. Li, S. Peng, and H. Ma, "Zero disturbance planning for space robots during target capture," in *Proc. IEEE Int. Conf. Contr. Autom.*, Xiamen, China, Jun. 2010, pp. 471–475.

[13] F. Aghili, "Optimal control of a space manipulator for detumbling of a target satellite," in *Proc. IEEE Int. Conf. Robot. Autom.*, Kobe, Japan, May 2009, pp. 3019–3024.

[14] T. Oki, S. Abiko, H. Nakanishi, and K. Yoshida, "Time-optimal detumbling maneuver along an arbitrary arm motion during the capture of a target satellite," in *Proc. IEEE/RSJ Int. Conf. Intell. Robot. Syst.*, San Francisco, CA, USA, Sep. 2011, pp. 625–630.

[15] Z.-W. Yu, X.-F. Liu, and G.-P. Cai, "Dynamics modeling and control of a 6-DOF space robot with flexible panels for capturing a free floating target," *J. Acta Astron.*, vol. 128, pp. 560–572, Nov./Dec. 2016.

[16] W. L. Xu and S. Yue, "Pre-posed configuration of flexible redundant robot manipulators for impact vibration alleviating," *IEEE Trans. Ind. Electron.*, vol. 51, no. 1, pp. 195–200, Feb. 2004.

[17] B. P. Larouche and Z. H. Zhu, "Autonomous robotic capture of non-cooperative target using visual servoing and motion predictive control," *Auto. Robots*, vol. 37, no. 2, pp. 157–167, 2014.

[18] R. A. McCourt and C. W. de Silva, "Autonomous robotic capture of a satellite using constrained predictive control," *IEEE/ASME Trans. Mechatronics*, vol. 11, no. 6, pp. 699–708, Dec. 2006.

[19] L. Zhang, Q. Jia, G. Chen, and H. Sun, "Pre-impact trajectory planning for minimizing base attitude disturbance in space manipulator systems for a capture task," *Chin. J. Aeronautics*, vol. 28, no. 4, pp. 1199–1208, 2015.

[20] S. Wolf *et al.*, "Variable stiffness actuators: Review on design and components," *IEEE/ASME Trans. Mechatronics*, vol. 21, no. 5, pp. 2418–2430, Oct. 2016.

[21] A. Jafari, N. G. Tsagarakis, B. Vanderborght, and D. G. Caldwell, "A novel actuator with adjustable stiffness (AwAS)," in *Proc. IEEE/RSJ Int. Conf. Intell. Robot. Syst.*, Taipei, Taiwan, Oct. 2010, pp. 4201–4206.

[22] R. Schiavi, G. Grioli, S. Sen, and A. Bicchi, "VSA-II: A novel prototype of variable stiffness actuator for safe and performing robots interacting with humans," in *Proc. IEEE Int. Conf. Robot. Autom.*, Pasadena, CA, USA, May 2008, pp. 2171–2176.

[23] G. Tonietti, R. Schiavi, and A. Bicchi, "Design and Control of a variable stiffness actuator for safe and fast physical human/robot interaction," in *Proc. IEEE Int. Conf. Robot. Autom.*, Barcelona, Spain, Apr. 2005, pp. 526–531.

[24] Y. Huang *et al.*, "Step length and velocity control of a dynamic bipedal walking robot with adaptable compliant joints," *IEEE/ASME Trans. Mechatronics*, vol. 18, no. 2, pp. 598–611, Apr. 2013.

[25] M. Grebenstein *et al.*, "The DLR hand arm system," in *Proc. IEEE Int. Conf. Robot. Autom.*, May 2011, pp. 3175–3182.

[26] B. Vanderborght, N. G. Tsagarakis, C. Semini, R. Van Ham, and D. G. Caldwell, "MACCEPA 2.0: Adjustable compliant actuator with stiffening characteristic for energy efficient hopping," in *Proc. IEEE Int. Conf. Robot. Autom.*, Kobe, Japan, May 2009, pp. 544–549.

[27] Z. Peng, J. Wang, and D. Wang, "Distributed containment maneuvering of multiple marine vessels via neurodynamics-based output feedback," *IEEE Trans. Ind. Electron.*, vol. 64, no. 5, pp. 3831–3839, May 2017.

[28] T. Li, Z. Li, D. Wang, and C. L. P. Chen, "Output-feedback adaptive neural control for stochastic nonlinear time-varying delay systems with unknown control directions," *IEEE Trans. Neural Netw. Learn. Syst.*, vol. 26, no. 6, pp. 1188–1201, Jun. 2015.

[29] B. Xu and F. Sun, "Composite intelligent learning control of strict-feedback systems with disturbance," *IEEE Trans. Cybern.*, to be published, doi: 10.1109/TCYB.2017.2655053.

[30] R. Storn and K. Price, "Differential evolution—A simple and efficient heuristic for global optimization over continuous spaces," *J. Global Optim.*, vol. 11, no. 4, pp. 341–359, 1997.

[31] N. Nasimul and I. Hitoshi, "Cellular differential evolution algorithm," in *Proc. 23rd Austral. Joint Conf. Artif. Intell.*, Adelaide, SA, Australia, 2010, pp. 293–302.

[32] Y.-W. Leung and Y. Wang, "An orthogonal genetic algorithm with quantization for global numerical optimization," *IEEE Trans. Evol. Comput.*, vol. 5, no. 1, pp. 41–53, Feb. 2001.

MING CHU was born in 1983. He received the Ph.D. degree from the Beijing University of Posts and Telecommunications (BUPT), Beijing, China, in 2010. He is currently an Associate Professor with the Automation School, BUPT. His recent research areas are flexible dynamics, nonlinear control, and robust control.

XINGYU WU was born in 1992. She is currently pursuing the master's degree with the School of Automation, Beijing University of Posts and Telecommunications, China. Her area of research covers flexible kinematic, dynamic modeling, and motion control of space manipulator.